C. R. Chimie 20 (2017) 540–548

Contents lists available at ScienceDirect

Comptes Rendus Chimie

www.sciencedirect.com

Full paper/Mémoire

Aluminum phosphate-based solid acid catalysts: Facile synthesis, characterization and their application in the esterification of propanoic acid with *n*-butanol

Boliang Liu, Pingping Jiang*, Pingbo Zhang, Hui Zhao, Jie Huang

Key Laboratory of Food Colloids and Biotechnology (Ministry of Education), School of Chemical and Material Engineering, Jiangnan University, Wuxi 214122, PR China

ARTICLE INFO

Article history:
Received 26 April 2016
Accepted 5 July 2016
Available online 22 February 2017

Keywords:
Sulfated aluminum phosphate
Esterification
Synthesis
Characterization
Catalytic performance

ABSTRACT

Novel solid acid catalysts synthesized from aluminum phosphate were prepared via a precipitation method and a subsequent sulfating treatment. Their catalytic performances for the esterification of propanoic acid with *n*-butanol were investigated. The as-prepared catalysts were characterized by means of X-ray diffraction (XRD), scanning electron microscopy (SEM), nitrogen adsorption–desorption, Fourier transform infrared spectroscopy (FT-IR), X-ray photoelectron spectroscopy (XPS), temperature programmed desorption of ammonia (NH_3-TPD), infrared spectroscopy of adsorbed pyridine, and other techniques. Experimental results of esterification reactions indicated that the calcination temperature can significantly affect the catalytic performances and the catalyst calcined at 500 °C (SO_4^{2-}/$AlPO_4$-500) exhibited the highest activity. The effects of different reaction conditions including reaction time, reaction temperature, catalyst amount and alcohol/acid molar ratio were studied in detail. The maximum propanoic acid conversion of 91% was achieved under optimum reaction conditions. Furthermore, the as-prepared SO_4^{2-}/$AlPO_4$-500 catalysts were tested for their reusability in repeated reaction cycles and could be effectively regenerated by a simple reactivation method.

1. Introduction

Esterification is a common and essential reaction for the synthesis of numerous fine chemicals such as perfumes, solvents, pharmaceuticals, food preservatives, cosmetics and biofuels [1,2]. As is widely known, acid catalysts are indispensable in esterification reactions. Conventional acid catalysts employed in industrial esterification processes are mainly homogeneous mineral acids (e.g., sulfuric acid), which possess high activities and low costs. However, the utilization of these mineral acids inevitably brings about some serious problems like the corrosion of equipment, the separation of catalyst and environmental contamination. Therefore, the replacement of these homogeneous acid catalysts by heterogeneous acid catalysts is highly necessary [3].

By comparison, solid acid catalysts have some advantages: they can be readily separated from liquid reaction mixtures, and they are environmentally friendly with respect to corrosiveness [4]. In recent years, various solid acid catalysts have been investigated for esterification reactions, including cation-exchange resins [5,6], zeolites [7,8], supported heteropolyacids [9,10], sulfate group promoted solid acids [11–13], oxides of elements with valence five or higher [14,15], carbon based solid acids [16,17] and biomass derived solid acids [18,19]. Among them, sulfate group promoted solid catalysts (mostly sulfated metal oxides) have drawn considerable attention in the field of solid acid catalysis [20–24].

* Corresponding author.
E-mail address: ppjiang@jiangnan.edu.cn (P. Jiang).

http://dx.doi.org/10.1016/j.crci.2016.07.006
1631-0748/

Owing to its superior properties, aluminum phosphate is regarded as a high-quality support material and has been applied in a variety of catalysis systems [25–28]. Amorphous aluminum phosphates commonly have high surface areas and large pore volumes. The skeleton of amorphous aluminum phosphate consists of tetrahedral units of AlO_4 and PO_4, which have a similar structure to that of silica [29]. This type of structure results in the high thermal stability of $AlPO_4$ [30]. All these above are believed to be vital properties for a catalyst support. In addition, the surface structural defects of $AlPO_4$ promote the formation of surface OH groups, which are similar to the Si–OH groups of zeolites. Thus an appropriate loading of heteroelements can remarkably enhance the catalytic performance of the $AlPO_4$ supported catalysts, due to their satisfactory dispersion and specific interactions with the support [31]. However, publications about $AlPO_4$ supported solid acid catalyst are rare in the literature [32]. Till now, to the best of our knowledge, investigations of sulfated aluminum phosphate solid acid used in esterification reactions have not been available. Moreover, acting as a support of solid acid, aluminum phosphate has a relatively lower cost compared with some frequently-used metal oxides such as ZrO_2 and TiO_2.

Accordingly, in the present work, amorphous aluminum phosphate was prepared and used as support for the immobilization of sulfate groups. Physicochemical properties of the resulting solid acid catalysts (SO_4^{2-}/$AlPO_4$-*T*) were investigated with the help of various characterization techniques. Catalytic activities of these catalysts were evaluated by the esterification of propanoic acid with *n*-butanol. The effects of esterification reaction parameters such as reaction time, reaction temperature, catalyst amount and molar ratio of alcohol to acid on the conversion of propanoic acid were studied in detail. Besides, recycling tests as well as reactivation of the catalyst were also performed.

2. Experimental

2.1. Preparation of catalyst

All chemicals in this study were of analytical grade and were used as received. Aluminum phosphate support was prepared via an incipient precipitation method under basic conditions. Typically, 15.01 g of $Al(NO_3)_3 \cdot 9H_2O$ and 4.61 g of H_3PO_4(85%) (corresponding to theoretical Al/P molar ratio of 1:1) were dissolved in 100 mL deionized water. To this solution, a diluted NH_3 solution (10 wt %) was added dropwise under vigorous stirring to attain a final pH of 9 and the resulting suspension was further stirred for 1 h. The precipitate was filtered, washed with deionized water to remove soluble impurities, and dried at 110 °C overnight. The thus obtained white solids were ground to fine powders in a carnelian mortar and calcined at 400 °C for 3 h. For targeted catalysts preparation, 0.8 g of the prepared $AlPO_4$ was added into a solution of 0.4 g $(NH_4)_2SO_4$ dissolved in 15 mL deionized water in a 50 mL beaker. After standing for 5 h at room temperature, this mixture was dried at 110 °C for 16 h and finally calcined at 400–550 °C for 3 h. The as-prepared catalysts were denoted as SO_4^{2-}/$AlPO_4$-*T*, where *T* denote the calcination temperature (°C).

2.2. Characterization of catalysts

The crystalline structure and phase composition of these prepared catalysts were analyzed by powder X-ray diffraction (XRD) technique on a Bruker AXS D8-Focus X-ray diffractometer equipped with a nickel filtered Cu Kα (0.15418 nm) radiation source and a scintillation counter detector. The XRD patterns were recorded by scanning the samples in a 2θ range of 3–60°. The morphologies and sizes were observed using a Hitachi S-4800 field emission scanning electron microscope (FE-SEM). Nitrogen adsorption–desorption measurements were performed at liquid nitrogen temperature (77 K), using a Micromeritics ASAP 2020 gas sorption analyzer. Specific surface areas were calculated from the linear part of adsorption data via the Brunauer–Emmett–Teller (BET) equation. The total pore volumes were estimated according to the adsorbance of nitrogen at a relative pressure (P/P_0) around 0.99. Fourier transform infrared (FT-IR) spectra of catalysts and the matrix were recorded on a Nicolet 6700 IR spectrometer in the spectral range of 2000–500 cm^{-1} with a resolution of 4 cm^{-1} using the conventional KBr pellet technique. Chemical states of the elements present on the catalyst surface were analyzed by X-ray photoelectron spectroscopy (XPS) on a Thermo ESCALAB 250 Xi instrument with monochromatized Al Kα line ($h\upsilon$ = 1486.6 eV) as the excitation source. Analyses were done at room temperature and the samples were maintained in a high vacuum (less than 10^{-8} Pa) to avoid noise in the spectra. The C 1s peak of hydrocarbon at 284.8 eV was used as an internal standard to which the binding energy values were referenced. The acidic properties of the catalysts were evaluated by temperature programmed desorption of ammonia (NH_3-TPD) using a Micromeritics AutoChem II 2920 instrument equipped with a TCD detector. Each sample was pretreated under a helium flow (50 mL/min) at 300 °C for 1 h and then cooled down to 100 °C. Subsequently, the sample was exposed to a flowing 10% NH_3/He gas mixture (50 mL/min) for 30 min. The excess physisorbed NH_3 was flushed out for 1 h with a pure helium gas flow. Measurements were conducted by heating the sample up to 650 °C with a ramping rate of 10 °C/min under a helium flow. To identify the Brønsted (B) and Lewis (L) acid sites on these catalysts, FT-IR spectra of pyridine adsorbed on the catalysts were recorded on a Nicolet 6700 spectrometer equipped with an in situ quartz cell. Before measurement, the sample was pretreated at 350 °C for 2 h in a vacuum of 10^{-2} Pa. After the quartz cell was cooled to room temperature, the sample was saturated with pyridine vapor. Excess physisorbed pyridine was removed by degassing for 30 min at room temperature under vacuum. The FT-IR spectrum of the adsorbed pyridine was then recorded. The quantities of acid sites present on the catalysts were estimated from the total amount of sulfate groups determined by an ion-exchange/titration method [33,34]. In a typical experiment, 0.30 g of catalyst and 3.0 g of NaCl, as an ion-exchange agent, were added into 60 mL of deionized water and stirred for 24 h. Afterwards, the solid was filtered. Using phenolphthalein as an indicator, the filtrate was titrated with 0.05 M NaOH solution. The amounts of acid sites were thus determined.

2.3. Catalytic activity test

The esterification reactions were performed in a 100 mL three-necked round bottom flask attached with a reflux condenser. This apparatus was placed on a magnetic-stirred oil bath maintained at a specified temperature. Propanoic acid, *n*-butanol and desired amount of catalyst were added into the reaction flask, the reaction was conducted under vigorous stirring. Various parameters of the reaction conditions, including reaction time, reaction temperature, catalyst amount (weight percentage of the reaction mixture), and the molar ratio of n-butanol to propanoic acid, have been optimized individually. After each batch reaction was terminated, the catalyst was immediately separated from the reaction mixture by filtration. The samples were drawn from the reaction mixture and analyzed by gas chromatography using a gas chromatograph (GC, SP-6890A) equipped with a FID detector and a capillary column (SE-54 30 m × 0.32 mm × 0.25 mm). Under the employed reaction conditions, butyl propionate was the predominant product detected (selectivity > 99%). The blank experiment was also carried out with no catalyst for comparison.

3. Results and discussion

3.1. Characterization

The XRD patterns of $SO_4^{2-}/AlPO_4$ catalysts calcined at different temperatures and $AlPO_4$ sample are shown in Fig. 1. The $AlPO_4$ support does not reveal any prominent diffraction peaks, indicating an amorphous phase. There are obvious characteristic peaks (2θ = 20.3°, 21.5°, 22.9° and 35.5°) of the orthorhombic α-$AlPO_4$ crystalline phase (JCPDS card no. 51-1674) observed for all the calcined $SO_4^{2-}/AlPO_4$ catalysts, indicating that the blend of $(NH_4)_2SO_4$ promotes the formation of orthorhombic α-$AlPO_4$ crystal. The $SO_4^{2-}/AlPO_4$-400 sample even exhibits clear peaks at 10.6°, 24.2°, 30.6° and 37.9°, respectively, corresponding to the diffraction of crystalline $NH_4Al(SO_4)_2$ (JCPDS card no. 23-0001). This implies that $(NH_4)_2SO_4$ contained in the catalyst precursor has not completely decomposed at this calcination temperature. When the calcination temperature further increases, the $NH_4Al(SO_4)_2$ crystalline phase tends to disappear. However, two new weak diffraction peaks (15.1° and 25.4°) assigned to crystalline $Al_2(SO_4)_3$ are identified for $SO_4^{2-}/AlPO_4$-450, $SO_4^{2-}/AlPO_4$-500 and $SO_4^{2-}/AlPO_4$-550 catalysts, which might be attributed to the interaction between excess SO_4^{2-} and metal ions during the calcination procedure. Similar phenomena were also observed in those SO_4^{2-}/M_xO_y solid acids [35–37].

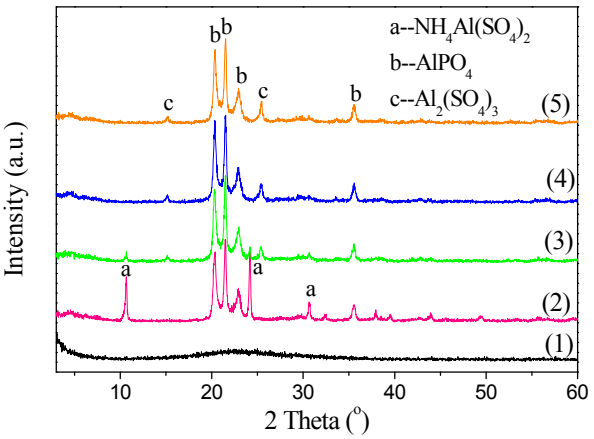

Fig. 1. XRD patterns of (1) $AlPO_4$; (2) $SO_4^{2-}/AlPO_4$-400; (3) $SO_4^{2-}/AlPO_4$-450; (4) $SO_4^{2-}/AlPO_4$-500; and (5) $SO_4^{2-}/AlPO_4$-550.

FE-SEM images displaying the surface morphologies of $AlPO_4$ support and the prepared $SO_4^{2-}/AlPO_4$ catalysts are shown in Fig. 2. As can be seen, catalyst support $AlPO_4$ shows the agglomerations of nanoparticles with irregular geometries (Fig. 2A). The incorporation of sulfate species on this support has yielded a $SO_4^{2-}/AlPO_4$ catalyst with large particle sizes and irregular shapes as shown in Fig. 2B. Besides, compared to bare $AlPO_4$, the as-prepared catalyst seems to have more porous structures. Actually, this is formed by the aggregation of numerous catalyst particles with larger sizes.

The textural properties of the catalysts and $AlPO_4$ support based on N_2 physical adsorption–desorption measurements are summarized in Table 1. It can be observed that the specific surface areas and pore volumes of the prepared $SO_4^{2-}/AlPO_4$ catalysts are evidently low compared to the support. This is due to the anchoring of sulfur species on the catalyst support resulting in the blockage of the pores as well as the sintering of $AlPO_4$ support during calcination (evidenced by XRD analysis). The relatively low surface areas and pore volumes of the catalysts may also have a high correlation with their larger particle sizes compared to bare $AlPO_4$ (see Fig. 2). Specific surface areas and total pore volumes of the as-prepared catalysts increased from 10.66 to 22.45 m^2/g and 0.035 to 0.071 cm^3/g, respectively, as the calcination temperature rose from 400 to 550 °C. These gradual changes well reflect the decomposition of $(NH_4)_2SO_4$ and the loss of sulfur species from the surface of catalysts along with the increase of calcination temperature.

Fig. 3 represents the FT-IR spectra of the $AlPO_4$ support and $SO_4^{2-}/AlPO_4$ catalysts of varied calcination temperatures. As can be discerned, the spectra of all samples exhibit broad absorption bands in the range of 1100–1130 cm^{-1}, which correspond to the asymmetric vibration of phosphate (triply degenerate P–O stretching vibration) [38]. For these prepared catalysts, it is noteworthy that the intensities of the bands (~1120 cm^{-1}) are markedly higher than that of the $AlPO_4$ support. Considering the overlapping between absorption bands of the P–O and S–O bonds, this may due to the additional asymmetric stretching vibration of the S–O bond associated with the incorporated sulfate groups. The spectra of these catalysts also show bands at 1385 cm^{-1}, which are assigned to the stretching vibration of S=O [39]. Hence, it can be concluded that the sulfate groups are covalently bonded to surface metal atoms of the $AlPO_4$. The surface sulfate groups are believed to be responsible for enhancing the acidity of the catalyst [40]. However, for $SO_4^{2-}/AlPO_4$-400 in particular, a weak peak at 1410 cm^{-1} identified in its spectrum reveals the presence of polynuclear sulfate $S_2O_7^{2-}$, namely ammonium pyrosulfate,

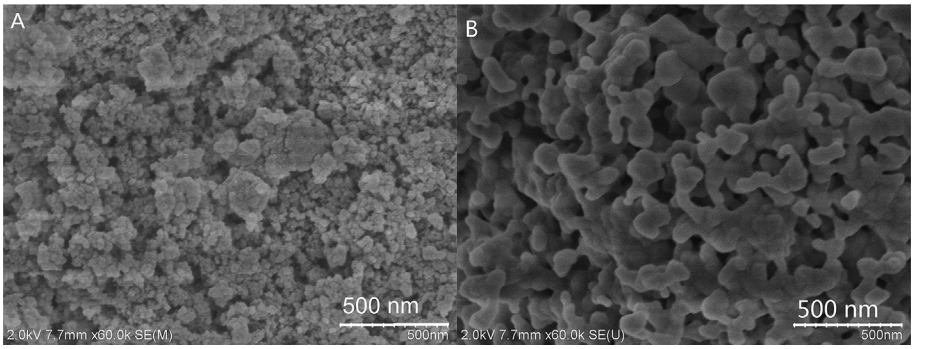

Fig. 2. Comparison between the SEM images of (A) $AlPO_4$ and (B) $SO_4^{2-}/AlPO_4$-500.

Table 1
Physico-chemical properties of the prepared samples.

Sample	A_{BET}[a] (m^2/g)	V_p[b] (cm^3/g)	Surface acid sites amount (mmol/g)	Surface acid sites density ($mmol/m^2$)
$AlPO_4$	152.16	0.678	—	—
$SO_4^{2-}/AlPO_4$-400	10.74	0.025	2.559	0.238
$SO_4^{2-}/AlPO_4$-450	13.66	0.039	2.404	0.176
$SO_4^{2-}/AlPO_4$-500	18.63	0.050	2.152	0.115
$SO_4^{2-}/AlPO_4$-550	22.45	0.071	2.009	0.089

[a] Specific surface area calculated by the BET method.
[b] Total pore volume estimated from nitrogen adsorbance at a relative pressure of 0.99.

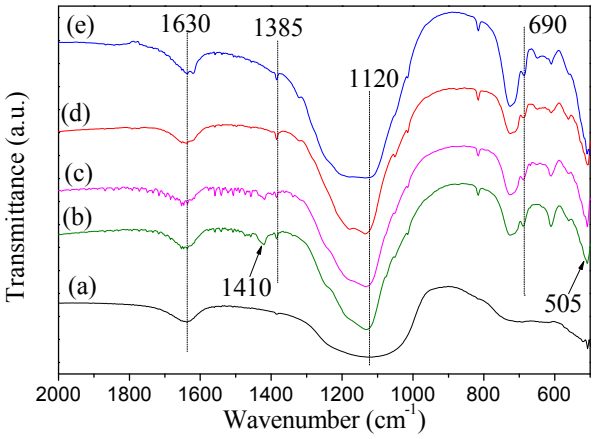

Fig. 3. FT-IR spectra of the prepared samples: (a) AlPO4; (b) $SO_4^{2-}/AlPO_4$-400; (c) $SO_4^{2-}/AlPO_4$-450; (d) $SO_4^{2-}/AlPO_4$-500; and (e) $SO_4^{2-}/AlPO_4$-550.

which is due to the incomplete decomposition of $(NH_4)_2SO_4$ [41]. This result is in line with the XRD analysis. The bands around 1630 cm^{-1} observed in all the spectra are attributed to the O–H bending vibration of the terminal –OH groups and absorbed water molecules present on the surface of the solids. Besides, the bands at ~690 cm^{-1} and 505 cm^{-1} for the catalysts are the Al–O–P stretching vibrations as well as the O–P–O bending mode of the PO_4^{3-} tetrahedral, respectively, indicating the presence of crystalline $AlPO_4$ that is also corroborated by the XRD analysis.

The scan spectra of the catalyst $SO_4^{2-}/AlPO_4$-500 drawn from XPS analysis are depicted in Fig. 4. The survey scan spectrum (Fig. 4a) reveals clear peaks of Al, P, S, C, and O elements. Therein, the observed peak of C 1s is due to carbon tape (i.e., internal standard) from the XPS instrument itself. There is also a faint peak of N 1s (around 400 eV) in the survey scan spectrum. This indicates that the $SO_4^{2-}/AlPO_4$-500 still contains traces of ammonium salt (i.e., $(NH_4)_2S_2O_7$), though not detected by the X-ray diffraction technique (Fig. 1). The detailed spectrum of Al 2p (Fig. 4b) shows one peak with binding energy at 75.4 eV, suggesting the presence of the Al^{3+} cation that results from the bonding of sulfate group [42]. As observed from the O 1s spectrum (Fig. 4c), the peak location at a binding energy of 532.7 eV can be attributed to surface O with chemical valence of −2, which is present in the phosphate matrix as well as surface sulfate groups [43]. Correspondingly, the peak at 169.6 eV is detected for the S 2p binding energy (Fig. 4d), which is assigned to sulfur with oxidation state of +6 contained in the catalyst [44]. The hexavalent sulfur is doubtlessly critical in the formation of the strong acid site [45,46]. The anchoring of these electron-drawing sulfur species to the $AlPO_4$ support would exacerbate the electron deficiency of surface Al atom, thus facilitating the formation of strong acidity. This result is in good accordance with the IR analysis. The surface sulfur content quantitatively estimated from the peak area of XPS spectrum is 4.79% (atomic ratio). In addition, the peak with binding energy around 134.6 eV found in P 2p spectrum (Fig. 4e) is ascribed to pentavalent phosphorus of PO_4 tetrahedral unit in the $AlPO_4$ skeleton [47].

The catalytic efficiency of a solid acid catalyst largely depends on its acidic properties, which can be evaluated by NH_3-TPD measurement. The NH_3-TPD profiles obtained for the prepared $SO_4^{2-}/AlPO_4$ catalysts are revealed in Fig. 5. There are various peaks observed in the measurement region of 100–650 °C, which correspond to desorption of NH_3 from the acid sites of different acid strength. The desorption temperature positively correlates with the strength of acid sites on the catalyst. The desorption profile of $SO_4^{2-}/AlPO_4$-400 catalyst primarily shows a broad peak centered at 280 °C in the range of 100–500 °C, indicating that the acid sites present on this catalyst are mainly weak and medium ones. This is probably due to the presence of residual $(NH_4)_2S_2O_7$ (verified by XRD and IR analysis) on the catalyst, which results from the incomplete decomposition of $(NH_4)_2SO_4$ and is unfavorable for the formation of strong

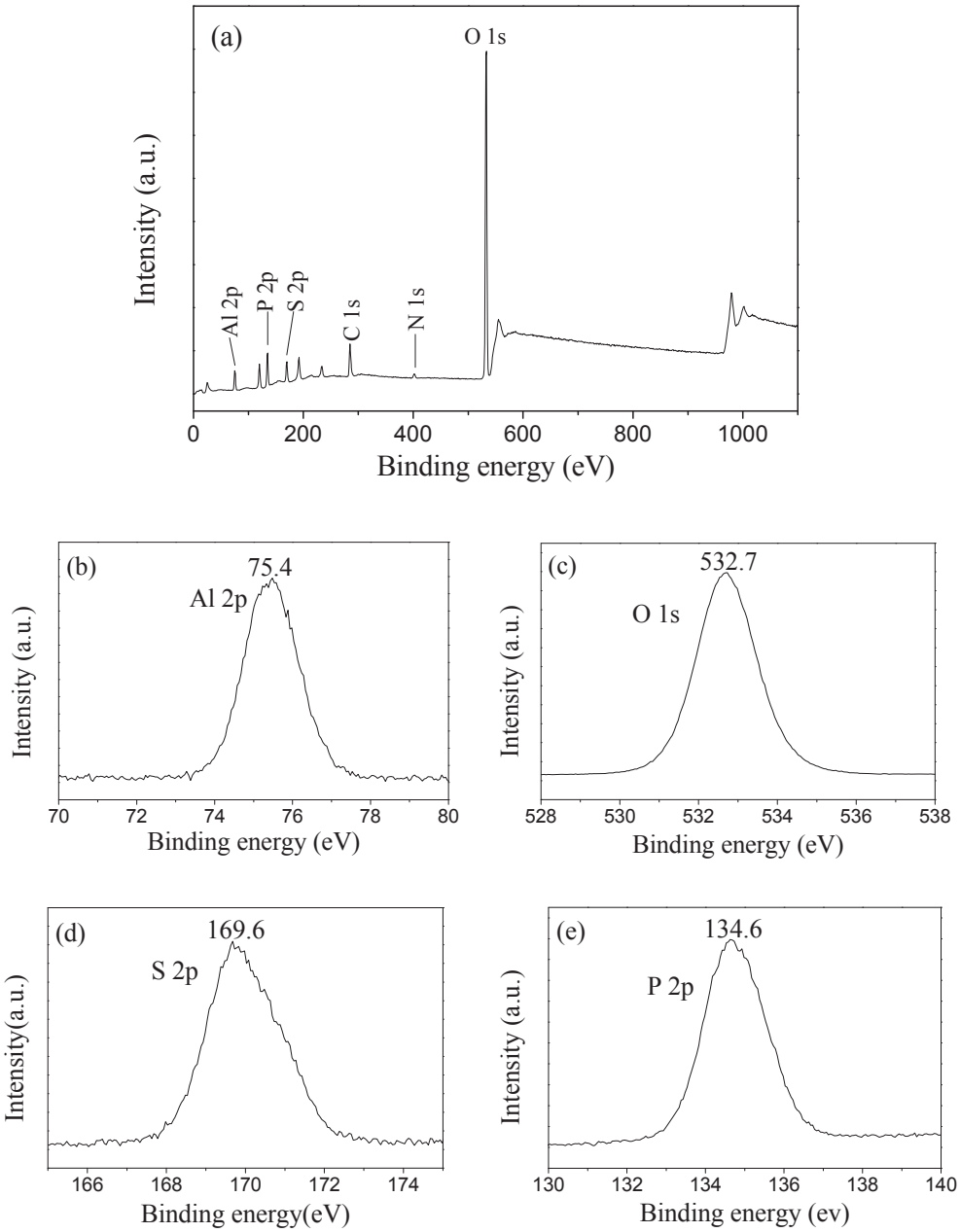

Fig. 4. XPS spectra of the $SO_4^{2-}/AlPO_4$-500: (a) survey scan spectrum and high-resolution spectra, (b) Al 2p, (c) O 1s, (d) S 2p, (e) P 2p.

acid site. In contrast, the TPD profiles of $SO_4^{2-}/AlPO_4$-450, $SO_4^{2-}/AlPO_4$-500, and $SO_4^{2-}/AlPO_4$-550 all exhibit the principal desorption peaks around 566 °C in a range of 450–620 °C, which can be assigned to strong acid sites. The covalent bonding of SO_4^{2-} to surface Al atoms of the $AlPO_4$ support and the strong electron-withdrawing effect of SO_4^{2-} are believed to be responsible for the generation of strong acidic active centers. It can be also noticed that the areas of the NH_3 desorption curves gradually decrease along with the increase of calcination temperature for all these catalysts. Since the area of the NH_3-TPD curve is in proportion to acid site amount of the corresponding catalyst, this reflects a gradual decline in total acid sites on these catalysts, which can be attributed to the decomposition of sulfur species present on the surface of the catalyst. This phenomenon is in line with the results based on the ion-exchange/titration method for the determinations of acid site content (see Table 1).

FT-IR spectra of pyridine adsorbed onto a solid surface can provide further insight into the nature of the surface acid sites. The resulting spectra for $SO_4^{2-}/AlPO_4$ catalysts are presented in Fig. 6. All the characteristic bands are revealed in the spectral region of 1400–1700 cm^{-1}. Covalently bonded pyridine (corresponding to Lewis acid sites)

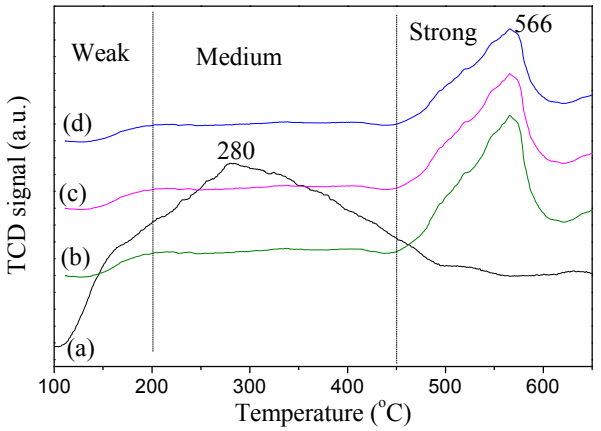

Fig. 5. NH_3-TPD profiles of the prepared catalysts: (a) $SO_4^{2-}/AlPO_4$-400; (b) $SO_4^{2-}/AlPO_4$-450; (c) $SO_4^{2-}/AlPO_4$-500; and (d) $SO_4^{2-}/AlPO_4$-550.

exhibits peaks at 1450 and 1616 cm^{-1} [48]. Bands at 1540 and 1640 cm^{-1} are assigned to pyridinium ion (pyridine adsorbed onto Brønsted acid sites) [49]. The bands centered at 1490 cm^{-1} in all spectra represent combined pyridine adsorbed on both Brønsted and Lewis acid sites [50]. Furthermore, the peaks around 1576 cm^{-1} can also be attributed to pyridine adsorbed onto Lewis acid sites [51]. These spectra revealed in Fig. 6 indicate the presence of both Brønsted and Lewis acid sites on the corresponding catalysts. It is worth noting that the band around 1640 cm^{-1} is absent only in the spectrum of pyridine adsorbed on the $SO_4^{2-}/AlPO_4$-400 catalyst. According to the weak and medium acidity of this catalyst (confirmed by NH_3-TPD analysis), the band at 1640 cm^{-1} may be associated with the presence of strong acid sites.

3.2. Catalytic performance

The conversions of propanoic acid are used to evaluate the efficiencies of the catalysts in esterification reactions and the results are listed in Table 2. For comparison, the catalytic performance of the $AlPO_4$ support and the result of blank esterification (without catalyst) are also included. As it can be seen, the $AlPO_4$ support shows almost negligible catalytic effect compared to the result of blank reaction. These results also indicate that the calcination temperature significantly affects the catalytic activity of these catalysts. Among the catalysts investigated, the $SO_4^{2-}/AlPO_4$-500 exhibits the highest catalytic activity. It is noteworthy that the $SO_4^{2-}/AlPO_4$-400 has evidently lower catalytic efficiency in comparison with other catalysts, despite the largest amount of acid sites it possesses. The results of NH_3-TPD and N_2 adsorption–desorption measurements reveal that the $SO_4^{2-}/AlPO_4$-400 possesses a predominantly weak and medium acidity and the lowest surface area (barely 10.74 m^2/g). In contrast, the NH_3-TPD profiles (Fig. 5) of the catalysts calcined at higher temperature (450 °C, 500 °C and 550 °C) verified the existence of strong acid sites on their surface, which are totally different from the $SO_4^{2-}/AlPO_4$-400. This is the main reason why these catalysts showed drastically higher catalytic efficiencies than the $SO_4^{2-}/AlPO_4$-400. Besides, the diffusion rate of the reaction substrate can also affect the catalytic activity of a solid catalyst. As the calcination temperature increased, the solid acid catalyst with the larger surface area (Table 1) may allow more facile diffusion of the reaction substrate; hence, the catalyst calcined at 500 °C was slightly more active than the one prepared at 450 °C. However, the catalytic activity decreases when the calcination temperature further increases. At excessively high calcination temperature, the decomposition of surface sulfate groups results in the loss of strong acid sites from the solid acid, thus undermining the activity of the solid acid.

Reaction parameters, such as reaction time, reaction temperature, catalyst amount and molar ratio of alcohol/acid, have considerable influences on the proceeding of esterification reaction. The effects of these reaction parameters were thus studied and the results are plotted in Fig. 7. The catalyst selected in these studies was $SO_4^{2-}/AlPO_4$-500, which possesses the best catalytic performance. Fig. 7a shows the effect of reaction time on the conversion of propanoic acid. Within the initial 3 h, the propanoic acid conversion witnessed a drastic growth and a final conversion of up to 91% is attained. Thereafter, the growth in the conversion almost stagnated, indicating the achievement of

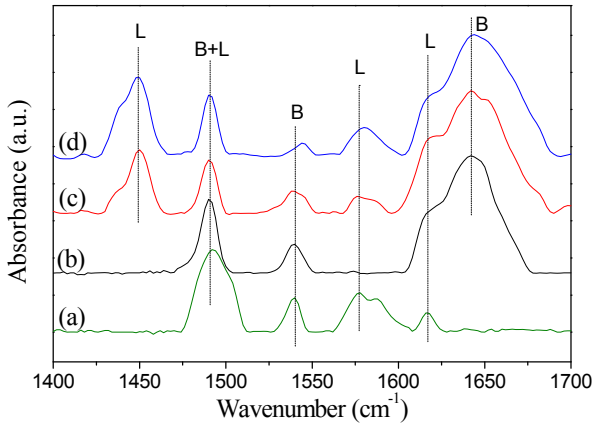

Fig. 6. FTIR spectra of pyridine absorbed on (a) $SO_4^{2-}/AlPO_4$-400; (b) $SO_4^{2-}/AlPO_4$-450; (c) $SO_4^{2-}/AlPO_4$-500; and (d) $SO_4^{2-}/AlPO_4$-550.

Table 2
Comparison of catalytic activity of different catalysts.

Catalyst	Conversion of propanoic acid (%)
$SO_4^{2-}/AlPO_4$-400	60.7
$SO_4^{2-}/AlPO_4$-450	85.9
$SO_4^{2-}/AlPO_4$-500	89.5
$SO_4^{2-}/AlPO_4$-550	79.2
$AlPO_4$	31.6
Blank	29.8
Recycling experiments of $SO_4^{2-}/AlPO_4$-500 catalyst	
Run 1	89.5
Run 2	81.6
Run 3	71.3
Run 4	64.7
Run 5	57.1

Reaction conditions: reaction temperature was 125 °C, reaction time was 150 min, molar ratio of *n*-butanol to propanoic acid was 1.5:1, and catalyst amount was 1.01 wt %.

equilibrium. A reaction time of 3 h is appropriate for the maximum conversion of propanoic acid.

The effect of reaction temperature on the esterification process is displayed in Fig. 7b. Apparently, the increase in the reaction temperature from 95 to 125 °C brought about a noticeable increase in the conversion of propanoic acid. It is well known that the esterification is an endothermic reaction, so a higher reaction temperature will facilitate the conversion of propanoic acid. However, a slight decrease in the conversion is observed as the reaction temperature increases beyond 125 °C. This can be ascribed to the vaporization of unreacted *n*-butanol at an excessively high temperature that far exceeds its boiling point (117 °C). The optimum temperature for this reaction should be determined at 125 °C.

Fig. 7c depicts the effect of catalyst amount on the conversion of propanoic acid. A nearly linear increase in the propanoic acid conversion from 64% to 89.5% can be observed by increasing the catalyst amount from 0.34 to 1.01 wt %. This may suggest that there are not enough active acid sites for the reaction with a relatively less catalyst amount and extra catalyst would enhance the reaction rate. Similar phenomena have been also observed in some other catalytic esterification reactions [52,53]. However, by further increasing the catalyst amount beyond 1.01 wt %, the conversion of propanoic acid tends to be constant owing to the limitation of the reaction equilibrium. Thus, a catalyst amount of 1.01 wt % is suitable for this esterification reaction.

The results of catalytic performances with various alcohol/acid molar ratios from 1:1 to 2:1 are demonstrated in Fig. 7d. As can be seen, the conversion of propanoic acid raised markedly from 74.1% to 89.5% when the alcohol/acid molar ratio increased from 1:1 to 1.5:1. Stoichiometrically, the molar ratio of alcohol to acid is 1:1 in the esterification reaction. Actually, a moderate excess of *n*-butanol is needed to promote the formation of the ester as the esterification reaction is reversible. Nevertheless, the further excess of alcohol may dilute carboxylic acid in the reaction mixture and flood the acid sites of the catalyst, which have adverse effects on the protonation of carboxylic acid at the acid sites, thus resulting in a decrease in the conversion of carboxylic acid [54,55]. Accordingly, there is a slight downward trend in the conversion of propanoic acid when the molar ratio exceeds 1.5:1. Hence, the alcohol/acid molar ratio of 1.5:1 is found to be optimal for this reaction.

In the reusability test, the SO_4^{2-}/$AlPO_4$-500 catalyst was subject to successive reaction cycles. After each batch reaction cycle, the catalyst was separated by filtration, washed with ethanol, dried at 80 °C in air, and then used in the following reaction cycle without any further reactivation. The results are presented in Table 2. As can be noted, the catalyst revealed a gradual decline in catalytic activity and the conversion of propanoic acid had fallen to 57.1% after five reaction cycles. This deactivation is probably due to the blockage of active acid sites with the reaction product molecules of ester and water adsorbed on the

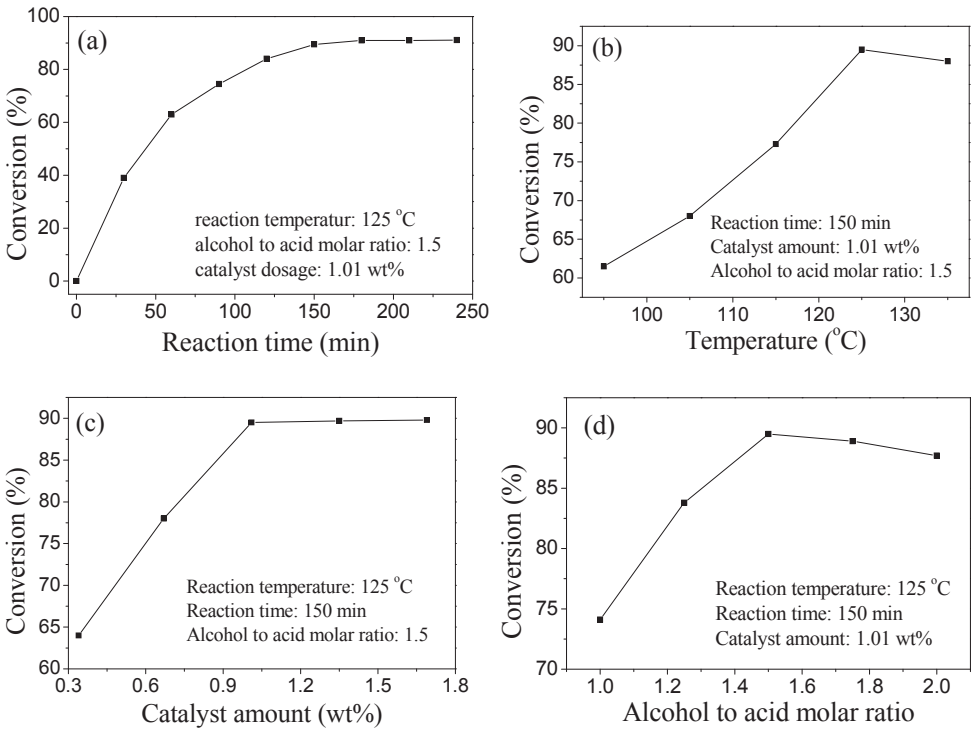

Fig. 7. Effects of (a) reaction time, (b) reaction temperature, (c) catalyst dose and (d) alcohol to acid molar ratio on the conversion of propanoic acid in catalytic esterification.

catalyst surface [56,57]. Furthermore, the acid site amount determined (by ion-exchange/titration method) for the recycled catalyst (after five reaction cycles) was 0.813 mmol/g, far less than that of the fresh catalyst (2.152 mmol/g). The NH_3-TPD profiles in Fig. 9 vividly elucidated this drastic change. The lessening in the amount of acid sites corresponds to the loss of surface sulfate groups, which is also responsible for the deactivation of the catalyst. Therefore, it is necessary to recover the catalytic activity of the spent $SO_4^{2-}/AlPO_4$-500 catalyst via a reactivation treatment. The recycled catalyst was immersed in a $(NH_4)_2SO_4$ solution (mass ratio of $(NH_4)_2SO_4$ to a recycled catalyst maintained 1:4, dried at 110 °C, and finally calcined at 500 °C. This reactivation method was proved to be effective as the reactivated catalyst exhibited a similar catalytic activity to the fresh sample (see Fig. 8). It can be clearly found from Fig. 9 that the reactivated catalyst has a NH_3-TPD curve similar to that of fresh $SO_4^{2-}/AlPO_4$-500, which accounts for its recovered activity.

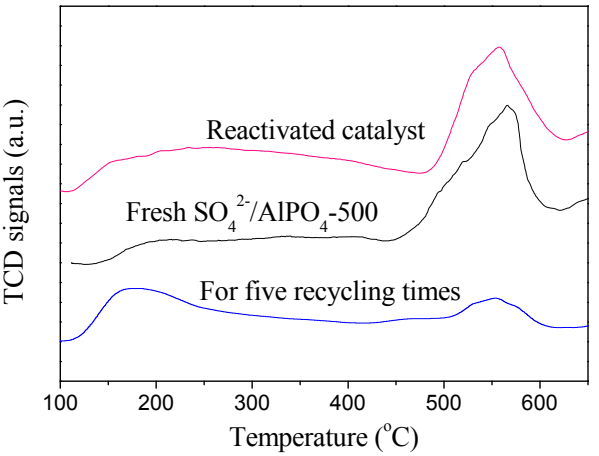

Fig. 9. NH_3–TPD curves of fresh, recycled and reactivated $SO_4^{2-}/AlPO_4$-500 catalysts.

4. Conclusion

A series of $SO_4^{2-}/AlPO_4$-*T* solid acid catalysts were prepared by a facile precipitation method and a subsequent surface sulfate modification. These catalysts were characterized in detail and applied in the esterification of propanoic acid with *n*-butanol. The calcination temperature was found to have an evident impact on the catalytic activities of these catalysts. The catalysts calcined at different temperatures have varied physicochemical properties including specific surface area, acid strength and total acid sites, which are key factors determining the catalytic activity of a solid acid. Among them, the $SO_4^{2-}/AlPO_4$-500 catalyst exhibited the highest activity. The maximum propanoic acid conversion of 91% can be achieved under the optimized reaction conditions: a reaction time of 3 h, a reaction temperature of 125 °C, a catalyst amount of 1.01 wt % and an alcohol/acid molar ratio of 1.5:1. Reusability tests revealed that the $SO_4^{2-}/AlPO_4$-500 suffers from an inevitable depletion in catalytic activity and a simple reactivation method was proposed. In summary, sulfated aluminum phosphate can be considered as a promising heterogeneous catalyst for acid catalyzed reactions.

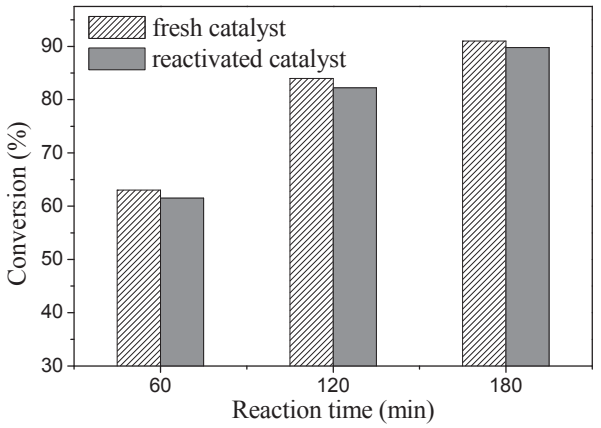

Fig. 8. Catalytic activity of fresh and reactivated $SO_4^{2-}/AlPO_4$-500. Reaction conditions: temperature was 125 °C, catalyst amount was 1.01 wt %, and the molar ratio of *n*-butanol to propanoic acid was 1.5:1.

Acknowledgements

The authors hereby acknowledge the financial support from the National Key Technology Research and Development Program (2012BAD32B03-4) and the Cooperative Innovation Foundation of Industry, Academy and Research Institutes (BY2013015-10) in the Jiangsu Province of China.

References

[1] M. Niederberger, G. Garnweitner, Chem. Eur. J. 12 (2006) 7282–7302.
[2] A. Aldana-Pérez, L. Lartundo-Rojas, R. Gómez, M.E. Niño-Gómez, Fuel 100 (2012) 128–138.
[3] F. Chen, H. Ma, B.J. Wang, J. Hazard. Mater. 147 (2007) 964–970.
[4] D.R. Fernandesa, A.S. Rochaa, E.F. Mai, C.J.A. Motab, V. Teixeira-da-Silva, Appl. Catal., A 425–426 (2012) 199–204.
[5] N. Boz, N. Degirmenbasi, D.M. Kalyon, Appl. Catal., B 165 (2015) 723–730.
[6] H.L. Zhang, J.C. Ding, Y.L. Qiu, Z.D. Zhao, Bioresour. Technol. 112 (2012) 28–33.
[7] S.S. Vieira, Z.M. Magriotis, M.F. Ribeiro, I. Graça, A. Fernandes, J.M.F.M. Lopes, S.M. Coelho, N.A.V. Santos, A.A. Saczk, Microporous Mesoporous Mater. 201 (2015) 160–168.
[8] K.Y. Nandiwale, V.V. Bokade, Chem. Eng. Technol. 38 (2015) 246–252.
[9] M. Kuzminska, T.V. Kovalchuk, R. Backov, E.M. Gaigneaux, J. Catal. 320 (2014) 1–8.
[10] A. Patel, V. Brahmkhatri, Fuel Process. Technol. 113 (2013) 141–149.
[11] G.C. Chen, F.B. Li, Z.J. Huang, C.Y. Guo, X.N. Qiu, H.B. Qiao, Z.C. Wang, S.B. Ren, W.F. Jiang, G.Q. Yuan, Fuel Process. Technol. 134 (2015) 11–17.
[12] M.Z. Wu, J.M. Guo, Y. Li, Y.J. Zhang, Ceram. Int. 39 (2013) 9731–9736.
[13] A. Patel, V. Brahmkhatri, N. Singh, Renew. Energy 51 (2013) 227–233.
[14] G. Mitran, T. Yuzhakova, I. Popescu, I.C. Marcu, J. Mol. Catal. A Chem. 396 (2015) 275–281.
[15] G. Mitran, O.D. Pavel, React. Kinet. Mech. Catal. 114 (2015) 197–209.
[16] X.Q. Gao, S.H. Zhu, Y.W. Li, Catal. Commun. 62 (2015) 48–51.
[17] Z.H. Gao, S.K. Tang, X.L. Cui, S.J. Tian, M.H. Zhang, Fuel 140 (2015) 669–676.
[18] J.M. Rafi, A. Rajashekar, M. Srinivas, B.V.S.K. Rao, R.B.N. Prasad, N. Lingaiah, RSC Adv. 5 (2015) 44550–44556.
[19] F. Ezebor, M. Khairuddean, A.Z. Abdullah, P.L. Boey, Bioresour. Technol. 157 (2014) 254–262.

[20] C.C. Huang, C.J. Yang, P.J. Gao, N.C. Wang, C.L. Chen, J.S. Chang, Green Chem. 17 (2015) 3609–3620.
[21] N. Kaur, A. Ali, Renew. Energy 81 (2015) 421–431.
[22] H. Zhao, P.P. Jiang, Y.M. Dong, M. Huang, B.L. Liu, New J. Chem. 38 (2014) 4541–4548.
[23] K. Saravanan, B. Tyagi, R.S. Shukla, H.C. Bajaj, Appl. Catal. B 172–173 (2015) 108–115.
[24] J.I. Moreno, R. Jaimes, R. Gómez, M.E. Niño-Gómez, Catal. Today 172 (2011) 34–40.
[25] Y. Danjo, I. Kikuchi, Y. Ino, M. Ohshima, H. Kurokawa, H. Miura, React. Kinet. Mech. Catal. 105 (2012) 381–389.
[26] J.W. Bae, S.M. Kim, S.H. Kang, K.V.R. Chary, Y.J. Lee, H.J. Kim, K.W. Jun, J. Mol. Catal. A Chem. 311 (2009) 7–16.
[27] M. Machida, K. Murakami, S. Hinokuma, K. Uemura, K. Ikeue, M. Matsuda, M. Chai, Y. Nakahara, T. Sato, Chem. Mater. 21 (2009) 1796–1798.
[28] S.C. Kishore, A. Pandurangan, Chem. Eng. J. 222 (2013) 472–477.
[29] F.M. Bautista, J.M. Campelo, A. Garcia, D. Luna, J.M. Marinas, A.A. Romero, G. Colon, J.A. Navio, M. Macias, J. Catal. 179 (1998) 483–494.
[30] K.V.R. Chary, G. Kishan, K. Ramesh, C.P. Kumar, G. Vidyasagar, Langmuir 19 (2003) 4548–4554.
[31] N.C. Masson, H.O. Pastore, Microporous Mesoporous Mater. 44–45 (2001) 173–183.
[32] W.L. Xie, D. Yang, Bioresour. Technol. 119 (2012) 60–65.
[33] H. Zhao, P.P. Jiang, Y.M. Dong, M. Huang, B.L. Liu, React. Kinet. Mech. Catal. 113 (2014) 445–458.
[34] T.T. Liu, Z.L. Li, W. Li, C.J. Shi, Y. Wang, Bioresour. Technol. 133 (2013) 618–621.
[35] H.P. Yan, Y. Yang, D.M. Tong, X. Xiang, C.W. Hu, Catal. Commun. 10 (2009) 1558–1563.
[36] J.C. Martín, S.B. Rasmussen, S. Suárez, M. Yates, F.J. Gil-Llambías, M. Villarroel, P. Ávila, Appl. Catal. B 91 (2009) 423–427.
[37] K.H. Jiang, D.M. Tong, J.Q. Tang, R.L. Song, C.W. Hu, Appl. Catal. A 389 (2010) 46–51.
[38] J.M. Campelo, M. Jaraba, D. Luna, R. Luque, J.M. Marinas, A.A. Romero, Chem. Mater. 15 (2003) 3352–3364.
[39] B.B. Chang, J. Fu, Y.L. Tian, X.P. Dong, Appl. Catal. A 437–438 (2012) 149–154.
[40] J.L. Ropero-Vega, A. Aldana-Pérez, R. Gómez, M.E. Niño-Gómez, Appl. Catal. A 379 (2010) 24–29.
[41] G.D. Yadav, A.D. Murkute, J. Catal. 224 (2004) 218–223.
[42] A.Q. Wang, X.L. Wu, J.X. Wang, H. Pan, X.Y. Tian, Y.L. Xing, RSC Adv. 5 (2015) 19652–19658.
[43] Q. Yu, X.J. Yao, H.L. Zhang, F. Gao, L. Dong, Appl. Catal. A 423–424 (2012) 42–51.
[44] Q. Yi, J. Zhang, X. Zhang, J. Feng, W. Li, Fuel 143 (2015) 390–398.
[45] C.W. Dunnill, Z.A. Aiken, A. Kafizas, J. Pratten, M. Wilson, D.J. Morgan, I.P. Parkin, J. Mater. Chem. 19 (2009) 8747–8754.
[46] L.G. Devi, R. Kavitha, Mater. Chem. Phys. 143 (2014) 1300–1308.
[47] R. Fu, L. Liu, W. Huang, P. Sun, J. Appl. Polym. Sci. 87 (2003) 2253–2261.
[48] M.J. López-Muñoz, R. van Grieken, J. Aguado, J. Marugán, Catal. Today 101 (2005) 307–314.
[49] R.V. Sharma, C. Baroi, A.K. Dalai, Catal. Today 237 (2014) 3–12.
[50] B. Mallesham, P. Sudarsanam, G. Raju, B.M. Reddy, Green Chem. 15 (2003) 478–489.
[51] V.C. dos Santos, K. Wilson, A.F. Lee, S. Nakagaki, Appl. Catal. B 162 (2015) 75–84.
[52] S. Kirumakki, N. Nagaraju, K. Chary, Appl. Catal. A 299 (2006) 185–192.
[53] B.R. Jermy, A. Pandurangan, Appl. Catal. A 288 (2005) 25–33.
[54] G. Kuriakose, N. Nagaraju, J. Mol. Catal. A Chem. 223 (2004) 155–159.
[55] Q. Shu, H. Yuan, B. Liu, L.H. Zhu, C.X. Zhang, J.F. Wang, Fuel 143 (2015) 547–554.
[56] J. Ni, F.C. Meunier, Appl. Catal. A 333 (2007) 122–130.
[57] K. Saravanan, B. Tyagi, H.C. Bajaj, Catal. Sci. Technol. 2 (2012) 2512–2520.